Contents lists available at ScienceDirect

Spectrochimica Acta Part A: Molecular and Biomolecular Spectroscopy

journal homepage: www.elsevier.com/locate/saa

Triphenyl-imidazole based reversible coloro/fluorimetric sensing and electrochemical removal of Cu²⁺ ions using capacitive deionization and molecular logic gates

G. Prabakaran [a], K. Velmurugan [a], R. Vickram [a], C. Immanuel David [a], A. Thamilselvan [b], J. Prabhu [a], R. Nandhakumar [a,*]

[a] Department of Applied Chemistry, Karunya Institute of Technology and Sciences (Deemed-to-be University), Karunya Nagar, Coimbatore 641 114, India
[b] Electro Organic-Division, Central Electrochemical Research Institute (CSIR-CECRI), Karaikudi 630 003, India

ARTICLE INFO

ABSTRACT

A simple hydroxyl-substituted triphenyl-imidazole based receptor (**HTPI**) which selectively detects Cu²⁺ ion by colorimetric and fluorimetric methods was developed. **HTPI** detects the Cu²⁺ ions with the absorption enhancement and fluorescence quenching by the possible ligand to metal charge transfer (LMCT) and the chelation-enhanced quenching (CHEQ) approaches, respectively. **HTPI** showed high selectivity and sensitivity for Cu²⁺ ions detection over other interfering and competing metal ions. Interestingly, **HTPI** detects Cu²⁺ ion (LOD) at nanomolar concentrations (19×10^{-9} M (UV–vis) & 27×10^{-9} M (fluorescence), respectively), which is lower than the permissible level of Cu²⁺ ion reported by World Health Organization (WHO). Furthermore, **HTPI** was applied to the molecular logic gate function by using chemical inputs, and Cu²⁺ ion was potentially removed (95%) via Capacitive Deionization technique.

© 2020 Elsevier B.V. All rights reserved.

1. Introduction

Over the years a wide range of colorimetric and fluorimetric sensors have been developed for the specific detection of environmentally and biologically important metal ions/anions [1–9]. Among them, copper is one of the third most abundant metal ion playing an important role in our daily life and thus used for various applications, such as printing, electrical manufacturing wires, medical equipment's etc. [10–14] As a result, copper can easily enter into drinking water and cause adverse effects to humans, animals and plants [15,16]. The over-accumulation of copper in our body leads to neurodegenerative diseases, including Alzheimer's and Wilson's disease, and its deficiency causes anemia [17–21]. The American Medical Association suggests that the presence of copper level in a normal human body should be 1.2–1.3 mg/day and our growth development is in the order of 0.1 mg/L. In addition, WHO also recommended that the allowed level of Cu²⁺ ions in drinking water be within 15–25 µM. Therefore, the development of coloro/fluorescent probes for the detection of Cu²⁺ in environmental/biological samples is getting more attention and highly demanding to date.

At present, there are many techniques introduced for the sensing of Cu²⁺, including Voltammetry, atomic absorption spectroscopy (AAS), inductively coupled plasma mass spectroscopy (ICP-MS), and colorimetric/fluorescent probe method (CFPM) [22–27]. In comparison, CFPM is one of the most frequently used technique to the sensing of Cu²⁺, due to its dual mode of detection, low cost, rapid response, accuracy, and high sensitivity [28]. So far, most of the chemosensors have been developed for the sensing of Cu²⁺ via either absorption or emission spectroscopy [29–31]. Recently, there are only a few literature reports for the detection of Cu²⁺ ions by both colorimetric and fluorimetric analysis, and also, it's highly challenging. Therefore, it is pivotal to develop a dual-channel coloro/fluorimetric probe for the detection of Cu²⁺ ion in an aqueous solution.

On the continuation of our previous work [32], we realized that hydroxyl-substituted probe is necessary for the selective sensing of Cu²⁺ ion. Accordingly, we have designed and synthesized the triphenyl imidazole derivatives **HTPI** and **TPI** by the treatment of benzil with salicylaldehyde and benzaldehyde, respectively. Probe **HTPI** comprising of benzil act as a fluorophore, and imidazole and phenolic –OH act as ionophores, thus separated by C—C single bond spacer. This probe was utilized for the sensing of metal ions via dual modes, i.e., UV–vis and fluorimetric, respectively, and compared with **TPI** (absence of -OH). Furthermore, **HTPI** was employed as a complexing agent for

* Corresponding author.
   E-mail address: nandhakumar@karunya.edu (R. Nandhakumar).

effective removal of Cu^{2+} ion via capacitive deionization method, and chemical inputs based logic gates were also demonstrated.

2. Experimental methods

2.1. Synthesis of **HTPI**

Salicylaldehyde (0.50 g, 4.09 mmol), benzil (2.14 g, 10.22 mmol), and ammonium acetate (2.52 g, 32.72 mmol) were dissolved in 30 ml of acetic acid in 100 ml round bottom flask. The reaction mixture was refluxed with vigorous stirring for 18 h and cooled to room temperature. The reaction mixture was poured into ice-cold water and the white precipitate formed was filtered, dried, and purified by column chromatography using petroleum ether – ethyl acetate as eluents. Yield: 78%. FT-IR ((KBr), (cm^{-1})): 1593, 3051 and 3197. ^{1}H NMR (200 MHz, CDCl$_3$, ppm): 7.55–7.58 (m, 4H), 7.25–7.48 (m, 8H), 7.0–7.10 (d, 1H), 6.91–6.94 (d, 1H). ^{13}C NMR (125 MHz, CDCl$_3$, ppm):157.5, 145.7, 130.5, 128.2, 128.1, 123, 127.3, 118.9, 117.8, 112.4. Elemental analysis: $C_{21}H_{16}N_2O$; calcd. (%); C, 80.75; H, 5.16; N, 8.97 and found (%); C, 80.70; H, 5.10; N, 8.90. LC-MS calcd.; $C_{21}H_{16}N_2O$: [M$^+$] 311.36, found; [M$^+$+H]$^+$ 312.40.
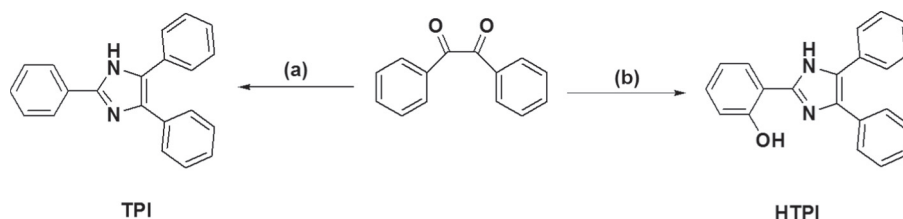
2.2. Synthesis of TPI

Similar procedure was followed for the synthesis of TPI. Yield: 78%, ^{1}H NMR (200 MHz, CDCl$_3$, ppm): 7.9–7.94 (m, 2H), 7.26–7.51 (m, 14H). Elemental analysis: $C_{21}H_{16}N_2$; calcd (%); C, 85.11; H, 5.44; N, 9.45, found (%); C, 85.00; H, 5.35; N, 9.35, LC-MS calcd.; for $C_{21}H_{16}N_2$: [M$^+$] 296.37, found; [M$^+$-H]$^+$ 295.49.

3. Results and discussion

3.1. Synthetic design of **HTPI** & TPI

Triphenyl-imidazole based probes **HTPI** and **TPI** were synthesized by a one-step simple condensation reaction between respective aldehydes (salicylaldehyde and benzaldehyde) and benzil in the presence of ammonium acetate, respectively as shown in Scheme 1. These probes were well-characterized by the spectroscopic and analytical techniques (Figs. S1–S5). For an efficient chemosensor, signalling and ion-binding units are highly indispensable. Accordingly, we have introduced the imidazole unit as an ionophore, where the presence of a donor nitrogen atom within the ring makes good interactions with metal ions [33–35]. Also, introducing the hydroxyl group on the phenyl ring covalently linked with conjugated imidazole-benzil scaffold provides a suitable coordination environment for the detection of Cu^{2+} ion by various photophysical pathways.

3.2. Colorimetric studies

3.2.1. Selectivity of **HTPI** towards Cu^{2+}

Initially, probe **HTPI** was treated with different solvents, such as THF, DMSO, and DMF, and studied their polarity by using UV–vis and fluorescence techniques (Fig. S15). From these results, **HTPI** showed the higher absorbance and emission intensities in THF than other solvents and thus used as a solvent for all the photophysical experiments. The UV–vis spectrum of **HTPI** (THF-H$_2$O, 1:1 v/v, solution HEPES = buffer, pH = 7.4) displayed two absorption bands at 236 nm and 321 nm, which were attributed to π-π* and n- π* transitions of the phenyl and imidazole rings. Upon the addition of Cu^{2+} to **HTPI**, a 6.2-fold enhancement of the absorption band intensity was observed, with a notable large blue shift (321 nm to 293 nm) in the absorption spectrum. Besides, the naked-eye observation showed that the colorless solution of **HTPI** instantly changed into sky blue color, which unquestionably proved that **HTPI** coordinates with Cu^{2+} ion in THF-H$_2$O solution. It is noteworthy to mention that the significant shift in the spectral wavelength assisted with the respective color changes are mainly due to the ligand to metal charge transfer (LMCT) process, thus resulting in a reduction of Cu^{2+} ions by **HTPI**. Furthermore, during the **HTPI** + Cu^{2+} complexation, the C—C single bond free rotation between the phenyl and imidazole scaffolds was arrested which eventually pushes the sensor into a different conformation making the molecule more rigid and causing a drastic absorption enhancement. Unfortunately, however, this complex did not exhibit a d-d band in the visible region and may be due to the high solvating nature. Under identical conditions, the addition of various cations to **HTPI** did not produce any significant spectral changes in the absorption spectrum except Hg^{2+} (Fig. 1a). When **HTPI** interacts with Hg^{2+}, the band intensity was slightly enhanced but there is no substantial color change in this solution. On the other hand, probe TPI did not exhibit any notable changes in the absorption bands with any of the metal ions (Fig. 1b). Therefore, these results advocated that the additional hydroxyl group substituted **HTPI** played a crucial role in the selective sensing of Cu^{2+} ion in THF-H$_2$O solution.

3.2.2. Competitive complexation experiment

To study the possible interaction of **HTPI** + Cu^{2+} complex with other competing metal ions (Ag$^+$, Al^{3+}, Ba^{2+}, Ca^{2+}, Cd^{2+}, Co^{2+}, Cr^{3+}, Ce^{3+}, Fe^{2+}, Fe^{3+}, Hg^{2+}, K$^+$, La^{3+}, Mg^{2+}, Mn^{2+}, Na$^+$, Ni^{2+}, Pb^{2+} and Zn^{2+}) interference experiments were performed. **HTPI** mixed with Cu^{2+} ion (100 equiv.) (Fig. 2) in the presence of same equivalents of other metal ions did not show any significant changes in the absorption band. This proved that there is no influence of other metal ions on the detection of Cu^{2+} ions. Hence, the probe **HTPI** selectively detects Cu^{2+} ion in the presence of other metal ions and can be potentially utilized for on-site monitoring works.
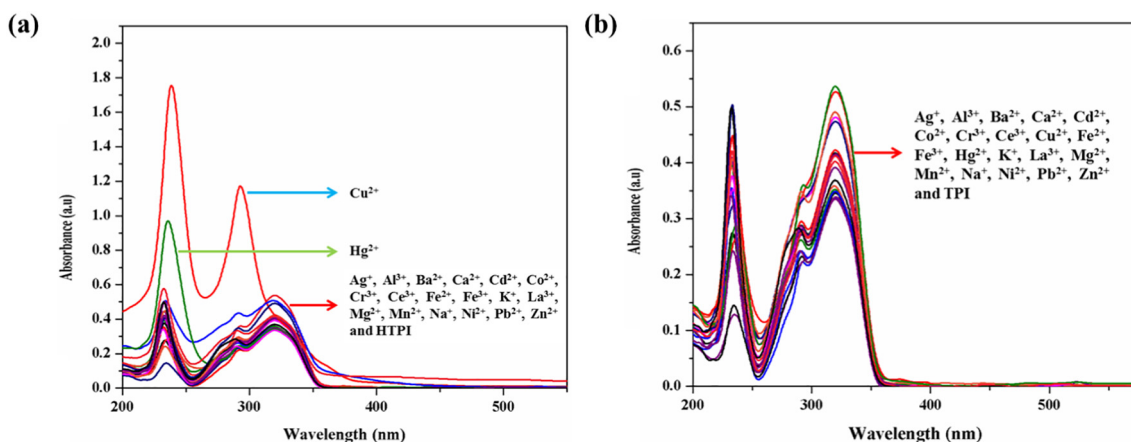

(a) Benzaldehyde, CH₃COONH₄, CH₃COOH, reflux, 18 h.
(b) Salicylaldehyde, CH₃COONH₄, CH₃COOH, reflux, 18 h

Scheme. 1. Synthesis of receptors **TPI** and **HTPI**. (a) Benzaldehyde, CH₃COONH₄, CH₃COOH, reflux, 18 h. (b) Salicylaldehyde, CH₃COONH₄, CH₃COOH, reflux, 18 h

Fig. 1. Absorption changes of the probes (a) **HTPI** and (b) **TPI** (4×10^{-5} M) in THF-H$_2$O (1:1 v/v, 50 mM (HEPES), pH = 7.4) in the presence of various metal ions (100 equiv.).

3.2.3. Binding stoichiometry

To get further insights into the binding stoichiometry between **HTPI** (host) and Cu^{2+} (guest), UV–vis titrations were performed in THF-H$_2$O (1:1 (v/v), HEPES 50 mM, pH = 7.4) solution. The absorbance of **HTPI** was gradually increasing by increasing the concentration of Cu^{2+} (0–100 equiv.) and associated with a large blue shift, got saturated during the addition of 100 equiv. of Cu^{2+}. This result indicated that **HTPI** has strong interactions with Cu^{2+} ions. Furthermore, to confirm the stoichiometric ratio of **HTPI**-Cu^{2+} (H-G) complex, Job's plot method was implemented and the maximum mole fraction was observed at 0.49 (Fig. 4), revealed a 1:1 binding stoichiometry between **HTPI** and Cu^{2+}. In addition, mass spectrum showed a prominent peak at 455.36 (m/z) for [**HTPI** + Cu^{2+} + NO$_3^-$ + H$_2$O] complex directly evidenced that 1:1 stoichiometric ratio between the **HTPI** and Cu^{2+} (Fig. S6).

To verify the binding stoichiometry and affinity, Benesi-Hildebrand method was performed for **HTPI**-Cu^{2+} complex by using the following equation [36].

$$\frac{1}{A - A_0} = \frac{1}{A' - A_0} + \frac{1}{Ka[A' - A_0]\left[Cu^{2+}\right]} \qquad (1)$$

where, A_0, A, and A' were represented as the absence, presence and saturated absorbance of Cu^{2+} with **HTPI**, and [Cu^{2+}] is the concentration of Cu^{2+} ion. Plotting of $1/A - A_0$ versus $1/$[Cu^{2+}] showed a linear

relationship, which also strongly supported the 1:1 complex stoichiometry of **HTPI** + Cu^{2+} (Fig. 3b), and the association constant (Ka) was calculated to be 9.84×10^4 M^{-1}. The LOD was found to be 19×10^{-9} M by using the equation 3δ/S, where δ denotes the standard deviation of the free probe, and S denotes the slope of the linear regression plot obtained from the titration spectrum [37].

3.2.4. Effect of pH, time and reversibility of HTPI

For practical utility, the effect of pH, time, and reversibility of the sensor plays a vibrant role in the selectivity of metal ions. Hence, the sensing ability of **HTPI** with Cu^{2+} ions was evaluated by different pH in THF-H$_2$O (1:1 v/v) solution. Though, at higher acidic and basic pH ranges, hydroxyl substituted **HTPI** could have been involved in the protonation and deprotonation processes, respectively, it did not much affect the absorbance intensity, and showed a weak absorption intensity in all the pH range. At the same time, surprisingly, in the case of **HTPI**-Cu^{2+} complex, absorption enhancement was observed in the wide range of pH (Fig. S7) and there were no notable changes in the intensity at the higher acidic and basic conditions. Therefore, **HTPI** detects Cu^{2+} ion in diverse pH ranges, and for our photophysical experiments, the physiological pH was selected as a working condition. The effect of time response for the complexation of **HTPI** with Cu^{2+} ion was monitored by UV–vis analysis (Fig. S8). It specified that the recognition of Cu^{2+} ions by **HTPI** accomplished within 2 min and persisted steadily
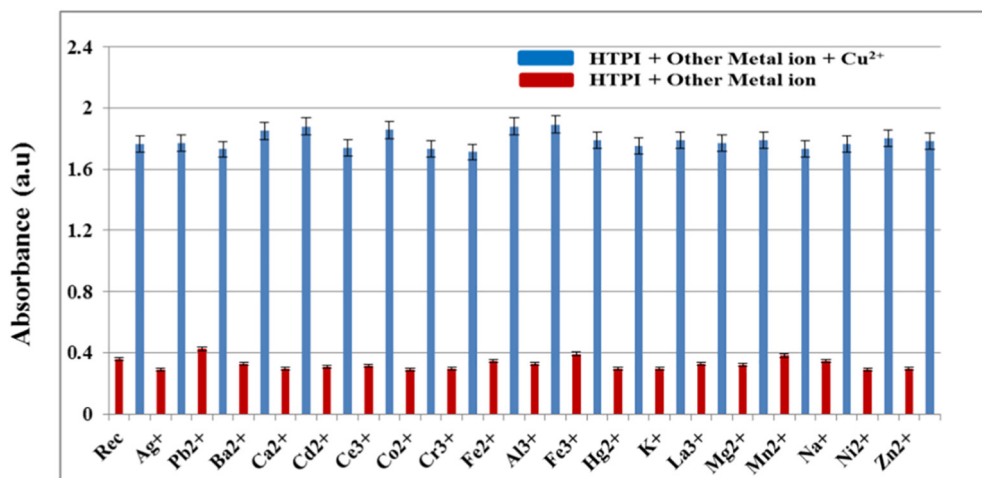

Fig. 2. Absorption changes of the **HTPI** with other metal ions (Cu^{2+} and other stated metal ions) in THF-H$_2$O (1:1 v/v, 50 mM (HEPES), pH = 7.4). The error bar suggests that the standard deviation of three measurements.
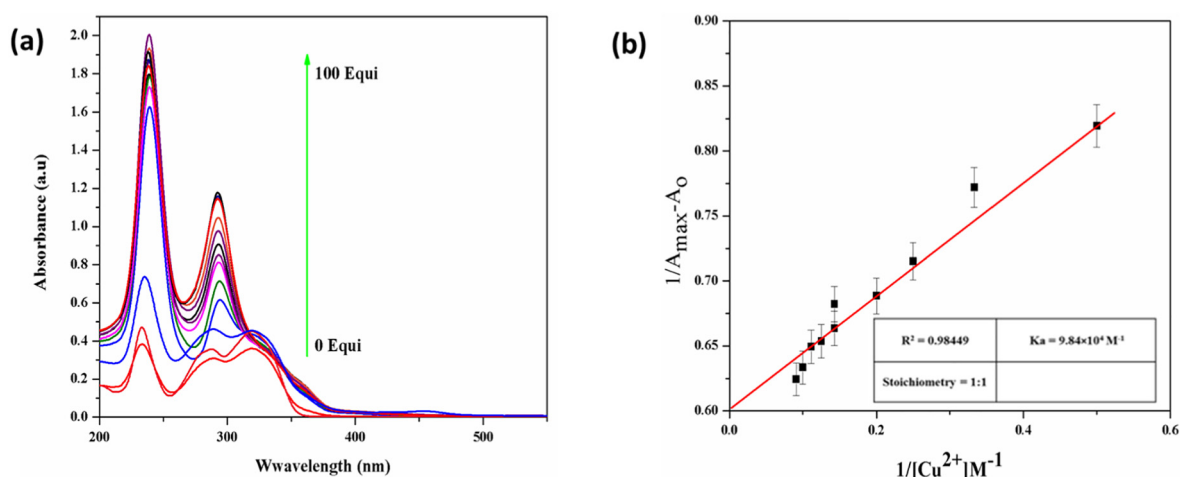
Fig. 3. (a) UV–vis spectrum of **HTPI** (4×10^{-5} M) in THF-H$_2$O (1:1 v/v, 50 mM (HEPES), pH = 7.4) with different concentrations (0–100 equiv.) of Cu^{2+}. (b) Benesi−Hildebrand non-linear curve fitting plot (absorbance at 236 nm) of **HTPI** assuming 1:1 binding stoichiometry with Cu^{2+}. The error bar suggests that the standard deviation of three measurements.

for a further 1 h and no changes in their intensity was noted even after a period of 24 h. Therefore, **HTPI** could be suitably utilized to detect Cu^{2+} ions in a short span of time. Besides, the reversibility of **HTPI** was investigated in the presence of Cu^{2+} and EDTA as shown in Fig. 5. As already discussed that **HTPI** showed the maximum absorbance in the presence of Cu^{2+} ion (100 equiv.), while introducing EDTA (100 equiv.) to **HTPI** + Cu^{2+} (100 equiv.) solution, the absorbance gets quenched and reached to the original **HTPI** signal, which is due to EDTA-Cu^{2+} complexation eventually displacing **HTPI** from coordination. Moreover, free **HTPI** again participates in the Cu^{2+} recognition process by the addition of Cu^{2+} ion in cyclic manners. The intensity almost remained the same upto fourteen cycles.

3.3. Fluorimetric studies

3.3.1. Metal ion selectivity

Based on the absorption spectrum, the excitation wavelengths of **HTPI** and **TPI** were fixed at 330 nm and 315 nm, respectively, and the emission studies were carried out. Free **HTPI** showed strong
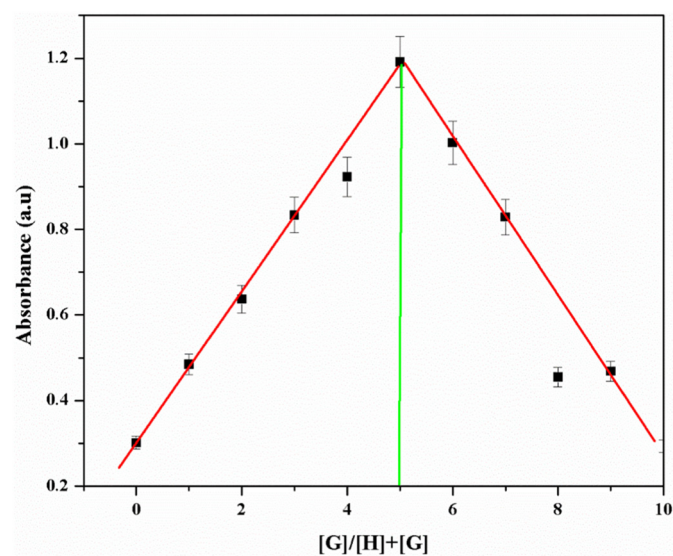

Fig. 4. Job's plot for the complexation of the [**HTPI** + Cu^{2+}] system in THF-H$_2$O (1:1 v/v, 50 mM (HEPES), pH = 7.4). The error bar suggests that the standard deviation of three measurements.

fluorescence intensity (436 nm) caused by its ionized form. Upon the addition of Cu^{2+} ions to **HTPI**, the fluorescence intensity got considerably quenched (3.4-fold) with a slight blue shift from 436 nm to 429 nm. This quenching process may possibly be due to the paramagnetic nature of Cu^{2+} ion and Chelation Enhanced Quenching (CHEQ) and are produced from charge transfer from **HTPI** to Cu^{2+} (LMCT) via reverse PET process. However, **HTPI** treated with other metal ions, such as Ag$^+$, Al^{3+}, Ba^{2+}, Ca^{2+}, Cd^{2+}, Co^{2+}, Cr^{3+}, Ce^{3+}, Fe^{2+}, Fe^{3+}, Hg^{2+}, K$^+$, La^{3+}, Mg^{2+}, Mn^{2+}, Na$^+$, Ni^{2+}, Pb^{2+} and Zn^{2+} did not produce the substantial changes in the emission spectra (Fig. 6a). Similarly, **TPI** was treated with all the above metal ions, and did not display considerable selectivity with any of the metal ions (Fig. 6b). These results indicated that the supplementary hydroxyl group substituted **HTPI** has contributed an essential part in Cu^{2+} binding process.

3.3.2. Competitive complexation experiment

Similar to colorimetric studies, competition experiments of **HTPI** were also carried out to investigate whether the other metal ions influence the sensing of Cu^{2+} ions via fluorimetric analysis. A fixed concentration of Cu^{2+} (100 equiv.) with **HTPI** was treated with an identical concentration of competing metal ions and their emission spectrum was monitored (Fig. 7). There were no significant changes in the emission spectra in the experiment carried out. Therefore, these results specified that the other potentially competing metals ions do not affect the sensing property of probe **HTPI** while detecting Cu^{2+} ion and hence the sensor could be utilized for practical purposes.

3.3.3. Binding stoichiometry

From the titration analysis, it was observed that the **HTPI** emission intensity gradually decreases by increasing the concentrations of Cu^{2+} and gets saturated at 100 equiv. of Cu^{2+}ions added, which prove that both **HTPI** and Cu^{2+} ion is involved in the chelation process. With the support of the Benesi-Hildebrand equation and fluorescence titrations, the association constant was found to be Ka = 1.98×10^4 M^{-1}. In addition, Job's plot of **HTPI**-Cu^{2+} showed a maximum mole fraction at 0.5, revealed a 1:1 (**HTPI**-Cu^{2+}) binding stoichiometry (Figs. 8b & 9). The limit of detection (LOD) was found to be 27×10^{-9} M [38], which is lower than the recommended level of Cu^{2+} ion in drinking water set by WHO. To evaluate the nature of quenching in **HTPI** by Cu^{2+} ion, the Stern-Volmer quenching constant (Ksv) was calculated to be 4.2467×10^4 M^{-1} (Fig. S9). It indicates that **HTPI** has a high binding affinity with Cu^{2+} ion leading to the static quenching of fluorescence. For more confirmation, **HTPI** and **TPI** quantum yield (φ) were calculated to be 0.14 and 0.09, and **HTPI** with Cu^{2+} was decreased to 0.03.
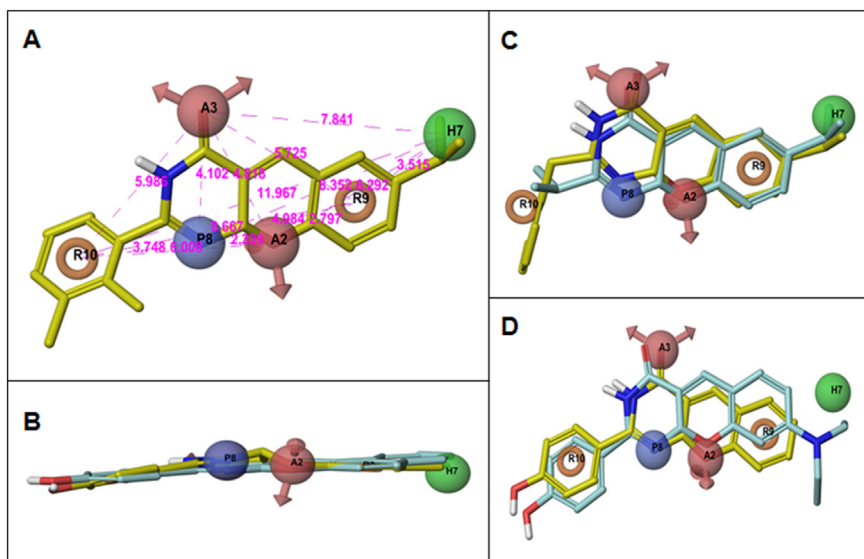
Fig. 5. UV–vis spectrum of **HTPI** (4×10^{-5} M) in THF-H$_2$O (1:1 v/v, 50 mM (HEPES), pH = 7.4) upon addition of Cu^{2+} (100 equiv.) and EDTA (100 equiv.).
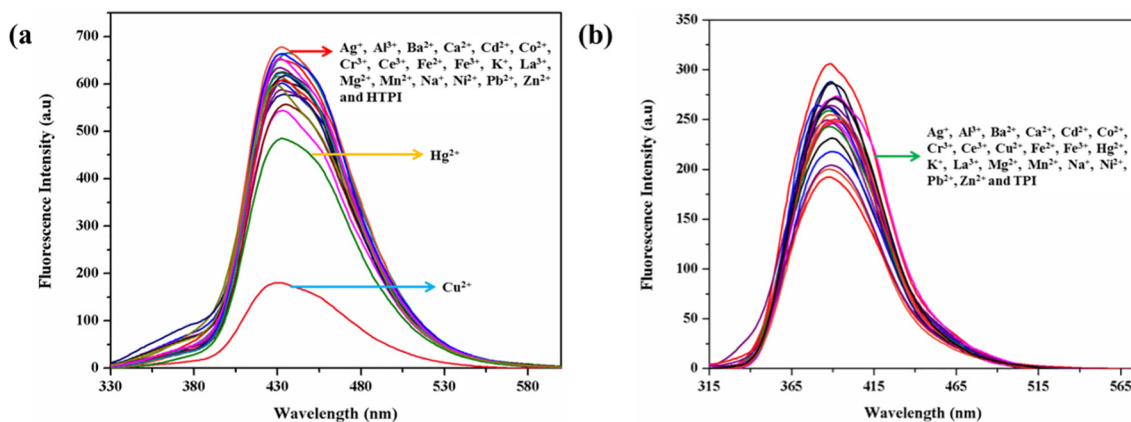

Fig. 6. Fluorescence spectra of (a) **HTPI** and (b) **TPI** (4×10^{-6} M) in the presence of various cations (100 equiv. λ_{ex} = 330 nm & λ_{ex} = 315 nm, respectively) in THF-H$_2$O (1:1 v/v, 50 mM (HEPES), pH = 7.4).

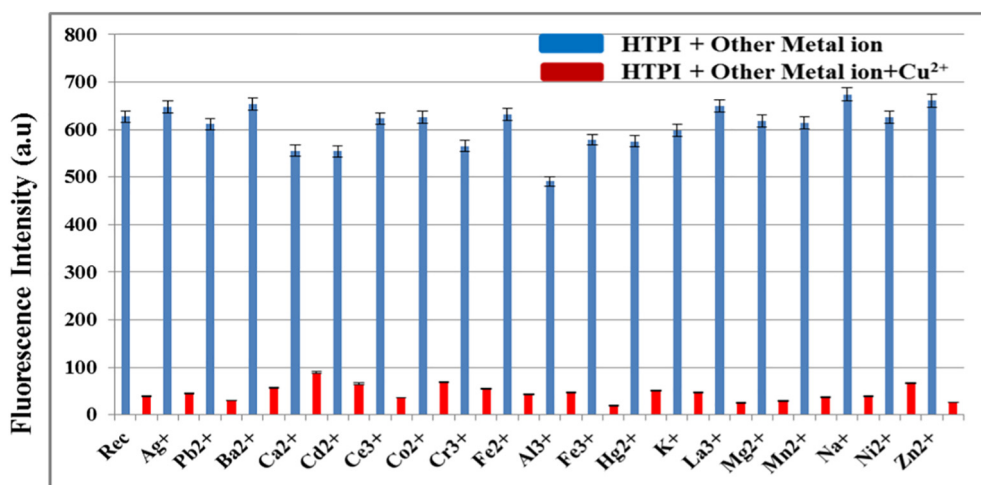**Fig. 7.** Fluorescence response of the **HTPI** + Cu^{2+} complex on addition of other metal ions (Ag$^+$, Al^{3+}, Ba^{2+}, Ca^{2+}, Cd^{2+}, Co^{2+}, Cr^{3+}, Ce^{3+}, Fe^{2+}, Fe^{3+}, Hg^{2+}, K$^+$, La^{3+}, Mg^{2+}, Mn^{2+}, Na$^+$, Ni^{2+}, Pb^{2+}, and Zn^{2+};100 equiv. λ_{ex} = 330 nm) in THF-H$_2$O (1:1 v/v, 50 mM (HEPES), pH = 7.4). The error bar suggests that the standard deviation of three measurement.
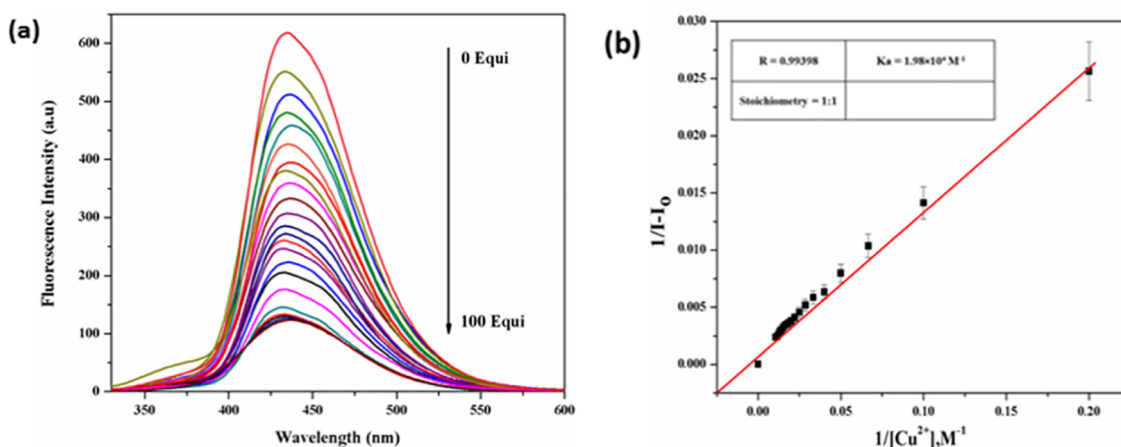
Fig. 8. (a) Fluorescence titration spectra of **HTPI** (4×10^{-6} M) upon the incremental addition of Cu^{2+} ions (0–100 equiv., $\lambda_{ex} = 330$ nm) in THF-H_2O (1:1 v/v, 50 mM (HEPES), pH = 7.4). (b) Benesi–Hildebrand plot of the 1:1 complex of **HTPI** and Cu^{2+} ions. The error bar suggests that the standard deviation of three measurements.

3.3.4. Effect of pH, time and reversibility

Fluorescence intensities of **HTPI** were quite stable in pH 6 to 8 and slightly changed in higher acidic and basic pH ranges, possibly due to protonation and deprotonation of hydroxyl substituted **HTPI**, respectively. In the case of **HTPI** + Cu^{2+} complex emission intensities were almost quenched and there are no observable changes in pH 5 to 9 (Fig. S10). Therefore, we have selected the physiological pH for all fluorimetric experiments. As a part of the experiments, the effect of time response of **HTPI** with Cu^{2+} ion was performed. The emission intensity of the probe **HTPI** was completely quenched within 7 min (Fig. S11) which indirectly proves that **HTPI** complex with Cu^{2+} in a short time. To know the reversibility of **HTPI**, an alternate addition of Cu^{2+} and EDTA were added into the solutions. Briefly, the addition of Cu^{2+} (100 equiv.) to **HTPI**, fluorescence intensity was decreased and the addition of EDTA (100 equiv.) to **HTPI** + Cu^{2+}, the intensity gets enhanced and reached to the original state of **HTPI** via EDTA-Cu^{2+} complexation effectively displacing the probe (Fig. 10). These results stated that **HTPI** assisted Cu^{2+} recognition process is reversible and could be used for many number of cycles.
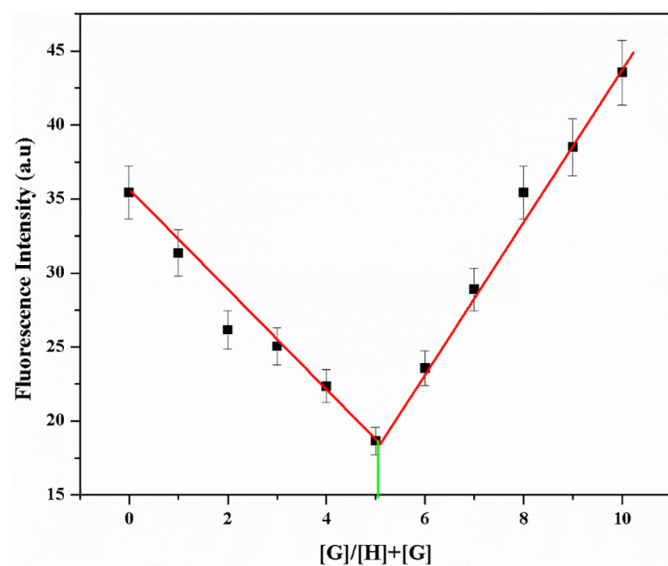
3.3.5. FT-IR and microscopic studies

FT-IR spectra of **HTPI** and **HTPI** + Cu^{2+} complex were recorded to get information about the mode of binding between the **HTPI** and Cu^{2+} ions. **HTPI** showed the characteristic absorption bands at 1593, 3051 and 3197 cm^{-1} corresponds to the imidazole C=N, secondary N—H, and phenyl -OH, respectively [39–41]. After the coordination of **HTPI** with Cu^{2+}, the absorption band was upward shifted to 1606 cm^{-1} and the other bands were almost disappeared. These changes specified that the **HTPI** containing C=N and -OH groups involved in the binding with Cu^{2+} ion (Fig. S14). To gain a better understanding of the surface topography changes, scanning electron microscopy (SEM) images of free **HTPI** and **HTPI**-Cu^{2+} were observed (Fig. 11). Eventually, free **HTPI** exhibited the rod-like structures stacked in order, which describes that the molecules are uniformly arranged. In the case of **HTPI**-Cu^{2+} complex displayed broken rod-like structures with irregular cubic particles have increased surface roughness. Therefore, based on the above studies, including colorimetric, fluorimetric studies, Job's plot, Benesi–Hildebrand non-linear curve fitting, mass spectra, and IR analysis, the proposed binding mechanism was
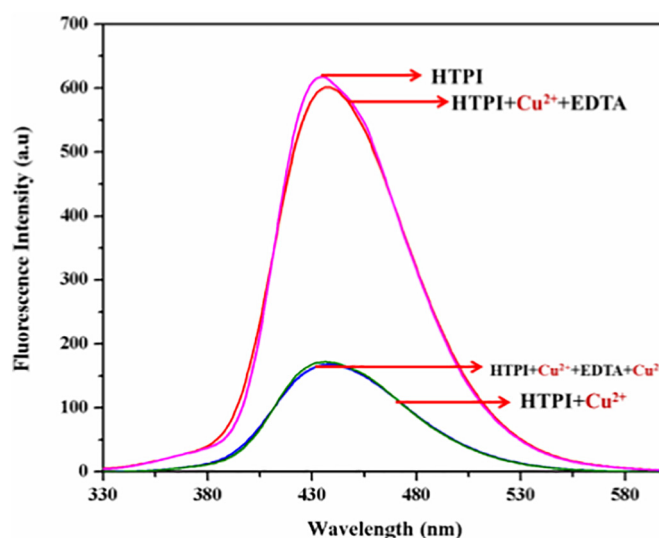

Fig. 9. Job's plot of **HTPI** with Cu^{2+} ions in THF-H_2O (1:1 v/v, 50 mM (HEPES), pH = 7.4). The error bar suggests that the standard deviation of three measurements.

Fig. 10. Fluorescence spectral changes of **HTPI** (4×10^{-6} M) in THF-H_2O (1:1 v/v, 50 mM (HEPES), pH = 7.4) on the addition of Cu^{2+} ions and EDTA (100 equiv. of each, $\lambda_{ex.} = 330$ nm).
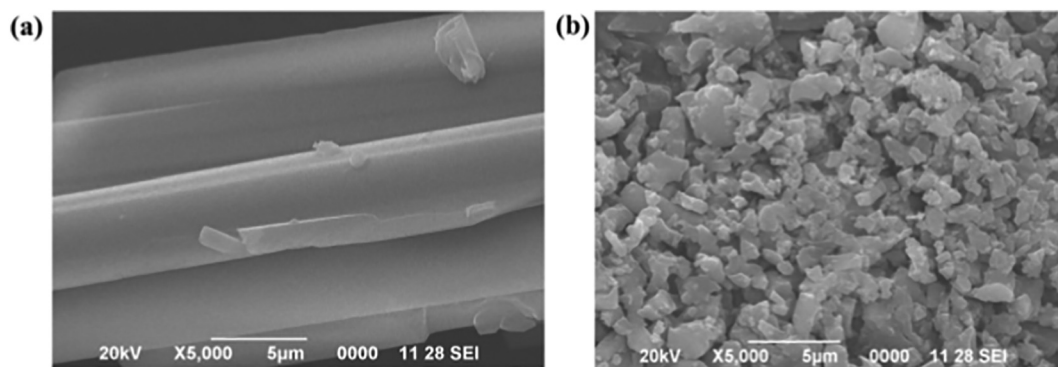
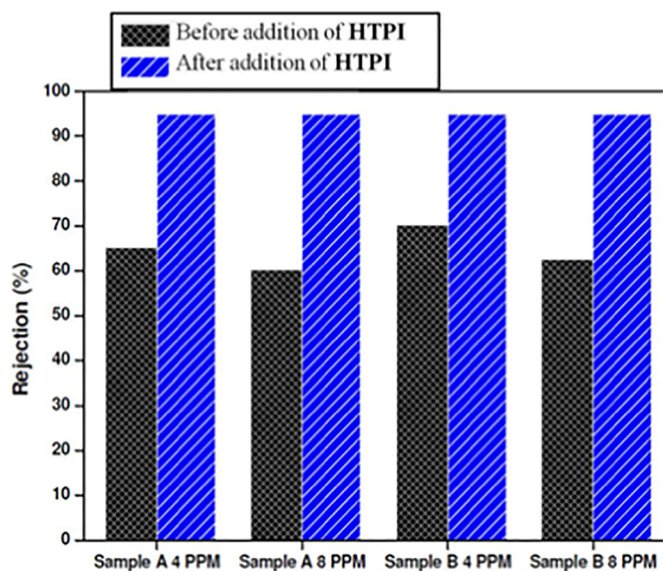**Fig. 11.** SEM images of a) **HTPI** and b) **HTPI** + Cu^{2+} (scale bar = 5 μm).

Fig. 12. Electrosorption performance of **HTPI** in the removal of Cu^{2+} by CDI process.

illustrated in the Scheme 2. When the chemosensor **HTPI** interacts with Cu^{2+}, there is an enhancement in the absorbance intensity assisted with a large blue shift. This may possibly be due to the LMCT process, thus resulting in a reduction of Cu^{2+} ion by **HTPI**. Also, carbon-carbon single bond free rotation between the phenyl and imidazole scaffold was blocked after the coordination, which eventually leads to a change in conformation of the complex and make the molecule more rigid which may be another reason for the absorption enhancement. On the other hand, during the **HTPI** interaction with Cu^{2+}, the fluorescence intensity was quenched and also associated by a slight shift in the emission profile, due to the paramagnetic nature of Cu^{2+} ions and CHEQ, produced due to the charge transfer from **HTPI** to Cu^{2+} (LMCT) via reverse PET processes [42–46]. As a result, **HTPI** displays turn "off-on" (colorimetric) and "on-off" (fluorimetric) mechanisms proposed based on the sensing of Cu^{2+} ions.

4. Application studies

4.1. Electrochemical removal of Cu^{2+} ions via capacitive deionization

Probe **HTPI** was potentially utilized to remove Cu^{2+} ions from the aqueous solution via Capacitive deionization (CDI) technique [47]. In

Fig. 13. Logic gate circuits of **HTPI** constructed by colorimetric and fluorimetric techniques.
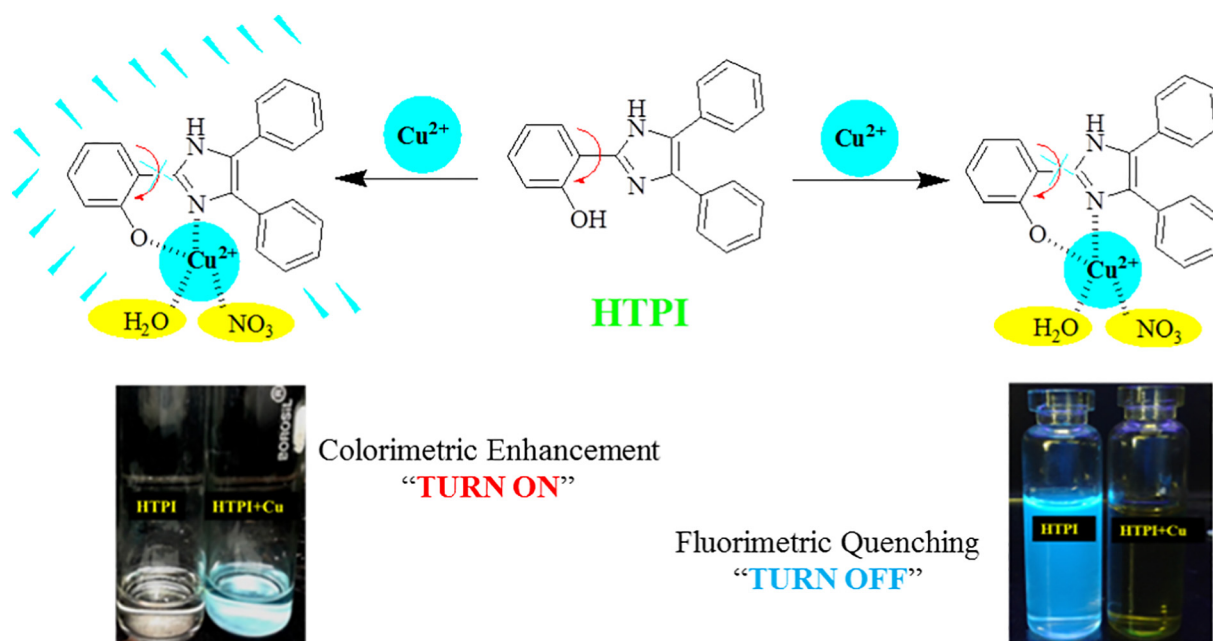
Scheme. 2. Plausible binding mechanism of **HTPI** with Cu^{2+}.

order to prove the removal efficiency, we have collected two different water samples, one from Karunya Nagar groundwater sample (Sample A), and the other one river water sample (Sample-B) from the Siruvani River, Coimbatore. These samples were spiked with $Cu(NO_3)_2$ solution concentrations of 4 and 8 ppm, respectively, and monitored their removal efficiency in the presence and absence of **HTPI** (2×10^{-5} M). The CDI containing the carbon aerogel electrodes exhibited the higher electrosorption capacitance even without the addition of **HTPI** (Fig. 12). In the absence of **HTPI**, both water samples showed moderate removal efficiency (62.5 to 70%) over Cu^{2+} ions, due to CDI containing carbon aerogel electrodes have higher electrosorption capacitance. In the presence of **HTPI** added water samples increased the rejection rate of Cu^{2+} ion to 95% (Table 1). These results suggested that **HTPI** could be played a vital role to remove Cu^{2+} from the contaminated river water and groundwater with an aid of CDI technique.

4.2. Molecular logic gate function

Based on the photophysical responses of **HTPI** towards Cu^{2+} and EDTA, we have constructed the IMPLICATION logic gate by both colorimetric and fluorimetric experiments. Here, Cu^{2+} and EDTA were used as two inputs, and the presence and absence of inputs are represented as "0" and "1", respectively. After the inclusion of Cu^{2+} and EDTA to **HTPI**, the absorbance and fluorescence intensities were used as outputs at 321 nm and 430 nm. For outputs, weak and strong fluorescence intensities were taken as "0" and "1", respectively. When inputs were (0,0) and (0,1), respectively the fluorescence intensity was extremely higher and the output was "1". Similarly, with the

inclusion of Cu^{2+} (1,0), fluorescence intensity was strongly quenched due to its binding with **HTPI** and output was "0". These results concluded that there is no signal activated in output when Cu^{2+} ion only present in this system. On the other hand, colorimetric responses were used as two inputs, such as Cu^{2+} and EDTA represents the INHIBIT logic function [48–50]. The absence and presence of inputs are represented as "0" and "1". For outputs, strong and weak absorptions were represented as "1" and "0", respectively. With inputs were (0, 0), (0, 1) and (1,1), respectively, there were no changes in the absorption and output was "0". With the addition of Cu^{2+} (1, 0), the absorption intensity was high due to its binding with **HTPI**, and output was "1" (Table 2 and Fig. 13).

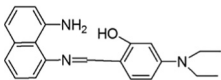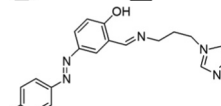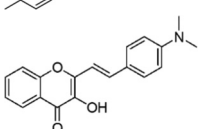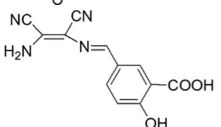Comparison of **HTPI** with recently reported chemosensors for Cu^{2+} (Table 3).
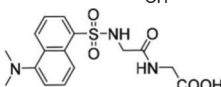
Table 2
Truth table of **HTPI** + Cu^{2+} complex.

		Truth table	
Input-1	Input-2	Output	
Cu^{2+}	EDTA	Fluorescence intensity at 430 nm (implication)	Absorbance at 321 nm (inhibit)
0	0	1	0
0	1	1	0
1	0	0	1
1	1	1	0

Table 1
Electrochemical removal of Cu^{2+} ion in carbon aerogel electrode with **HTPI** (2×10^{-5} M).

Samples	Amount of Cu^{2+} present in blank solution (ppm)	Amount of Cu^{2+} in permeate (ppm)		Rejection (%)	
		Before addition of **HTPI**	After addition of **HTPI**	Before addition of **HTPI**	After addition of **HTPI**
Sample-A	4	1.4	0.2	65	95
Sample-A	8	3.2	0.4	60	95
Sample-B	4	1.2	0.2	70	95
Sample-B	8	3	0.4	62.5	95

Table 3
Comparison of **HTPI** with recently reported chemosensors for Cu^{2+}.

Compound	Mode of detection	Detected ions	Detection medium	K_a (M^{-1})	Detection limit	Interfering ions	Ref
	Colorimetric and fluorimetric	Cu^{2+}	DMSO/H_2O (3:7)	$5.7 \times 10^4\ M^{-1}$ & $1.5 \times 10^4\ M^{-1}$	9.52×10^{-9} M & 15.1×10^{-9} M	Fe^{2+}	[42]
	Fluorimetric	Cu^{2+}	MeOH/H_2O (7:3)	–	1.8×10^{-6} M	–	[51]
	Colorimetric and fluorimetric	Cu^{2+}	Water	–	8×10^{-6} M & 5.7×10^{-7} M	–	[52]
	Fluorimetric	Cu^{2+}	CH_3CN-HEPES (1:9)	$7.63 \times 10^9\ M^{-2}$	2.19×10^{-7} M	–	[53]
	Fluorimetric	Cu^{2+}	HEPES BUFFER SOLUTION	$3.09 \times 10^4\ M^{-1}$	0.29×10^{-6} M	–	[54]
HTPI	Colorimetric and fluorimetric	Cu^{2+}	THF-Water (1:1)	$9.84 \times 10^4\ M^{-1}$ & $1.98 \times 10^4\ M^{-1}$	19×10^{-9} M & 27×10^{-9} M	Hg^{2+}	(This work)

5. Conclusion

In summary, we have designed and synthesized a hydroxyl-substituted triphenyl-imidazole based probe **HTPI**, which detects Cu^{2+} ions at nanomolar concentrations by dual-channel colorimetric and fluorimetric methods. The **HTPI** interactions with Cu^{2+} displayed an enhanced absorbance (6.2-fold) followed by a significant blue shift caused by LMCT, thus resulting in a reduction of Cu^{2+} ion by **HTPI** along with the arresting of the C—C single bond rotation between imidazole and phenyl rings during the **HTPI**-Cu^{2+} complex. On the other hand, **HTPI**-Cu^{2+} complex drastically quenches the fluorescence (3.4-fold) because of the paramagnetic nature of Cu^{2+} ion and CHEQ via reverse PET process. Furthermore, the static nature of quenching mechanism was proved by Stern-Volmer plot, which displayed the strong interaction between **HTPI** and Cu^{2+} ion. The binding stoichiometry was found to be 1:1 between the **HTPI** and Cu^{2+} ion, and the association constants were calculated as Ka = $9.84 \times 10^4\ M^{-1}$ and Ka = $1.98 \times 10^4\ M^{-1}$, by colorimetric and fluorimetric analysis, respectively. **HTPI** was successfully used to remove Cu^{2+} ions by Capacitive Deionization technique, and chemical inputs based molecular logic gates were illustrated. Therefore, **HTPI** based colorimetric/fluorimetric sensor can be used for the naked-eye detection of Cu^{2+} ions in environmental monitoring applications.

Author information

G.P., K.V. & R.N. – Design, synthesis, and characterization of the sensor along with writing, discussion, and revising the manuscript. R.V, C·I, & J.P- are taking part in the photometric studies, discussion, and revising manuscript.

A.T – performed the capacitive deionization studies and related discussions. All authors were involved in the writing, revising, and the completion of the manuscript.

Declaration of competing interest

No conflict of interest exists.

Acknowledgement

Appendix A. Supplementary data

UV–Vis, pH, time response, NMR, Mass spectra, Mass spectra for Complex are given in supporting information. Supplementary data to this article can be found online at https://doi.org/10.1016/j.saa.2020.119018.

References

[1] J.A.C. Jr, A.T. Aron, K.M. Ramos-Torres, C.J. Chang, Chem. Soc. Rev. 44 (2015) 4400–4414.
[2] C. Immanuel David, N. Bhuvanesh, J. Haritha, A. Thamilselvan, D. Parimala devi, A. Abiram, J. Prabhu, R. Nandhakumar, ACS Omega 5 (6) (2020) 3055–3072.
[3] J. Prabhu, K. Velmurugan, A. Raman, N. Duraipandy, M.S Kiran, S. Easwaramoorthi, L. Tang, R. Nandhakumar, Anal. Chim. Acta 1090 (2019) 114–124.
[4] H. Lia, X. Suna, T. Zhenga, Z. Xub, Y. Songc, X. Gua, Sens. Actuators B Chem. 279 (2019) 400–409.
[5] G. Yin, T. Niu, Y. Gan, T. Yu, P. Yin, H. Chen, Y. Zhang, H. Li, S. Yao, Angew. Chem. Int. Ed. 57 (2018) 4991–4994.
[6] N.K. Hien, D.T. Nhan, W.Y. Kim, M.V. Bay, P.C. Nam, D.U. Van, I.-T. Lim, J.S. Kim, Dyes Pigments 152 (2018) 118–126.
[7] L. Tang, Z. Zheng, Z. Huang, K. Zhong, Y. Biana, R. Nandhakumar, RSC Adv. 5 (2015) 10505–10511.
[8] K. Velmurugan, J. Prabhu, L. Tang, T. Chidambaram, M. Noel, S. Radhakrishnan, R. Nandhakumar, Anal. Methods 6 (2014) 2883–2888.
[9] K. Velmurugan, A. Raman, S. Easwaramoorthi, R. Nandhakumar, RSC Adv. 4 (2014) 35284–35289.
[10] R. Kumar, H. Jain, P. Gahlyan, A. Joshi, C.N. Ramachandran, New J. Chem. 42 (2018) 8567–8576.
[11] N. Fredj, J.S. Kolar, D.M. Prichard, T.D. Burleigh, Corros. Sci. 76 (2013) 415–423.
[12] A.T. Ozyılmaz, N. Colak, M.K. Sangun, M. Erbil, B. Yazıcı, Prog. Org. Coat. 54 (2015) 353–359.
[13] A. Taher, Appl. Mech. Matter 799 (2015) 222–231.
[14] N. Nanjundan, R. Narayanasamy, S. Geib, K. Velmurugan, R. Nandhakumar, M.D. Balakumaran, P. Thangavelu Kalaichelvan, Polyhedron 110 (2016) 203–220.
[15] K. Yin, B. Li, X. Wang, W. Zhang, L. Chen, Biosens. Bioelectron. 64 (2015) 81–87.
[16] A.P.S. Gonzales, M.A. Firmino, C.S. Nomura, F.R.P. Rocha, P.V. Oliveira, I. Gaubeur, Anal. Chim. Acta 636 (2009) 198–204.
[17] J. Mandala, P. Ghoraia, K. Palb, P. Karmakarb, A. Sahaa, J. Lumin. 205 (2019) 14–22.

[18] E. Gaggelli, H. Kozlowski, D. Valensin, G. Valensin, Chem. Rev. 106 (2006) 1995–2044.

[19] P.G. Welsh, J. Lipton, C.A. Mebane, J.C.A. Marr, Ecotoxicol. Environ. Saf. 69 (2008) 199–208.

[20] K.J. Barnham, C.L. Masters, A.I. Bush, Nat. Rev. Drug Discov. 3 (2004) 205–214.

[21] H. Wang, S. Zhao, Y. Xu, L. Li, B. Li, M. Pei, G. Zhang, J. Mol. Struct. 1203 (2020) 127384–127399.

[22] J.P. Lafleur, R. Lam, H.M. Chan, E.D. Salin, J. Anal. At. Spectrom. 20 (2010) 1315–1317.

[23] Z. Zhu, Z. Liu, H. Zheng, S. Hu, J. Anal. At. Spectrom. 25 (2010) 697–703.

[24] H.N. Kim, W.X. Ren, J.S. Kim, J. Yoon, Chem. Soc. Rev. 41 (2012) 3210–3244.

[25] Z.X. Wang, Y.-X. Guo, S.-N. Ding, Microchim. Acta 182 (2015) 2223–2231.

[26] P. Sianglam, S. Kulchat, T. Tuntulani, W. Ngeontae, Spectrochim. Acta, Part A 183 (2012) 408–416.

[27] K.J.A. Kundig, R.D. Weed, Copper and Copper Alloys, Mechanical Engineers' Handbook, John Wiley & Sons, Inc., 2014

[28] S. Saha, S. Das, P. Sahoo, Chemistry Select 4 (2019) 13968–13973.

[29] R. Konecna, S. Fintova, Copper Alloys-Early Applications and Current Performance-Enhancing Processes, In Tech 2012.

[30] N. Narayanaswamy, T. Govindaraju, Sensors Actuators B Chem. 161 (2012) 304–310.

[31] M.M.H. Khalil, A. Shahat, A. Radwana, M.F. El-Shahat, Sens. Actuators B Chem. 233 (2016) 272–280.

[32] L. Tang, N. Wang, Q. Zhang, J. Guo, R. Nandhakumar, Tetrahedron Lett. 54 (2013) 536–540.

[33] A.P. de Silva, H.Q.N. Gunaratne, T. Gunnlaugsson, A.J.M. Huxley, C.P. McCoy, J.T. Rademacher, T.E. Rice, Chem. Rev. 97 (1997) 1515–1566.

[34] X. Xie, S. Acc, Chem. Res. 29 (1996) 598–606.

[35] S.I. Hazarika, A.K. Atta, Comptes Rendus Chimie 22 (2019) 599–613.

[36] H.A. Benesi, J.H. Hildebrand, J. Am. Chem. Soc. 71 (1949) 2703–2707.

[37] K. Velmurugan, R. Vickram, R. Karthick, C.V. Jipsa, S. Suresh, G. Prabakaran, J. Prabhu, G. Velraj, R. Nandhakumar, J. Photochem. Photobiol. A Chem. 401 (2020) 112737.

[38] X. Cao, Q. Gao, X. He, Y. Bai, W. Sun, Luminescence (2019) 1–8.

[39] K. Nakanishi, Infrared Absorption Spectroscopy-Practical, Holden-Day, Inc., San Francisco, 1962.

[40] R.M. Silverstein, G.C. Bassler, T.C. Morrill, John Wiley and Sons, New York, (1981).

[41] K. Velmurugan, A. Thamilselvan, R. Antony, V.R. Kannan, L. Tang, R. Nandhakumar, J. Photochem. Photobiol. A Chem. 333 (2017) 130–141.

[42] Z. Guo, Q. Niu, T. Li, E. Wang, Tetrahedron 75 (2019) 3982–3992.

[43] D.S. Huerta-José, J.G. Hernández-Hernández, C.A. Huerta-Aguilar, P. Thangarasu, Sens. Actuators B Chem. 293 (2019) 357–365.

[44] J.A.O. Granados, P. Thangarasu, N. Singh, J.M. Vázquez-Ramos, Food Chem. 278 (2019) 523–532.

[45] C.A. Huerta-Aguilar, T. Pandiyan, N. Singh, N. Jayanthi, Spectrochim. Acta Part A 146 (2015) 142–150.

[46] C.A. Huerta-Aguilar, T. Pandiyan, P. Raj, N. Singh, R. Zanella, Sens. Actuators B Chem. 223 (2016) 59–67.

[47] D. Derin, K. Velmurugan, J. Prabhu, N. Bhuvanesh, A. Thamilselvan, R. Nandhakumar, Spectrochim. Acta A 174 (2017) 62–69.

[48] L. Feng, Z. Lyu, A. Offenhausser, D. Mayer, Angew. Chem. Int. Ed. 54 (2015) 7693–7697.

[49] Y.-M. Zhang, W. Zhu, W.-J. Qu, H.-L. Zhang, Q. Huang, H. Yao, T.-B. Wei, Q. Lin, J. Lumin. 202 (2018) 225–231.

[50] S. Uchiyama, N. Kawai, A. Prasanna de Silva, K. Iwai, J. Am. Chem. Soc. 126 (2004) 3032–3033.

[51] S. Slassi, M. Aarjane, A. Ghayoury, A. Amine Spectrochim. Acta, Part A 215 (2019) 348–353.

[52] Y. Hu, A. Chen, Z. Kong, D. Sun, Molecules 24 (2019) 4283.

[53] N. Jiang, X. Gong, T. Zhong, Y. Zheng, G. Wang, J. Mol. Struct. 1219 (2020) 128573.

[54] Y. Wang, J. Zhou, L. Zhao, B. Xu, Dyes Pigments 180 (2020) 108513.